Published online 25 January 2017 *Nucleic Acids Research, 2017, Vol. 45, No. 7* **4255–4268**
doi: 10.1093/nar/gkx044

RNA binding and chaperone activity of the *E. coli* cold-shock protein CspA

Enrico Rennella[1,2,3], Tomáš Sára[4], Michael Juen[5], Christoph Wunderlich[5], Lionel Imbert[1,2,3], Zsofia Solyom[1,2,3], Adrien Favier[1,2,3], Isabel Ayala[1,2,3], Katharina Weinhäupl[1,2,3], Paul Schanda[1,2,3], Robert Konrat[4], Christoph Kreutz[5] and Bernhard Brutscher[1,2,3,*]

[1]Institut de Biologie Structurale, Université Grenoble 1, 71 avenue des Martyrs, 38044 Grenoble Cedex 9, France, [2]Commissariat à l'Energie Atomique et aux Energies Alternatives (CEA), Grenoble, France, [3]Centre National de Recherche Scientifique (CNRS), Grenoble, France, [4]Department of Computational & Structural Biology, Max F. Perutz Laboratories, Campus, Vienna Biocenter 5, A-1030 Vienna, Austria and [5]Institute of Organic Chemistry, University of Innsbruck, Innrain 80/82, 6020 Innsbruck, Austria

Received November 14, 2016; Revised January 11, 2017; Editorial Decision January 13, 2017; Accepted January 17, 2017

ABSTRACT

Ensuring the correct folding of RNA molecules in the cell is of major importance for a large variety of biological functions. Therefore, chaperone proteins that assist RNA in adopting their functionally active states are abundant in all living organisms. An important feature of RNA chaperone proteins is that they do not require an external energy source to perform their activity, and that they interact transiently and non-specifically with their RNA targets. So far, little is known about the mechanistic details of the RNA chaperone activity of these proteins. Prominent examples of RNA chaperones are bacterial cold shock proteins (Csp) that have been reported to bind single-stranded RNA and DNA. Here, we have used advanced NMR spectroscopy techniques to investigate at atomic resolution the RNA-melting activity of CspA, the major cold shock protein of *Escherichia coli*, upon binding to different RNA hairpins. Real-time NMR provides detailed information on the folding kinetics and folding pathways. Finally, comparison of wild-type CspA with single-point mutants and small peptides yields insights into the complementary roles of aromatic and positively charged amino-acid side chains for the RNA chaperone activity of the protein.

INTRODUCTION

Ribonucleic acids (RNAs) fulfill a variety of essential functions in the cell, ranging from the transfer of genetic information, the catalysis of chemical reactions, to the regulation of cellular processes. Most RNA molecules have to adopt well-defined secondary and tertiary structures in order to be able to perform their cellular functions. *In vitro*, RNAs often fold into a variety of different conformations with similar free energies. Also during transcription RNA molecules can get trapped in kinetically favored non-active conformations. Therefore, *in vivo*, most RNAs are assisted in their folding process by a variety of chaperone proteins that help the RNA to reach the thermodynamically most favorable native conformation by lowering the energetic barriers between competing conformational states. Examples of proteins with reported RNA chaperone activity are ribosomal proteins, heterogeneous nuclear ribonuclear proteins (hnRNPs), cold shock domain proteins, bacterial histone-like proteins, SM-like proteins and viral nucleocapsid and core proteins (1–3). An important feature of RNA chaperone proteins is that they do not require adenosine triphosphate (ATP) or any other chemical energy source for their activity, and that they interact transiently and non-specifically with their RNA targets. So far, little is known about the mechanistic details of the RNA chaperone activity of these proteins, although models have been proposed for the RNA chaperone activity of StpA (4) and HIV-1 NC proteins (5).

Cold-shock proteins (CSPs) are small proteins of about 70 amino acids, that are ubiquitous in Eubacteria and Archaea, and that are transiently induced under cold stress conditions to fulfill various cellular functions. CSPs are also homologous to the cold shock domain (CSD) of Eucaryotic Y-box proteins, which are involved in transcriptional and translational regulation. CspA is the major cold-shock protein of *Escherichia coli*, with expression levels that can reach 10% of the total protein synthesis during cold adaptation, with intracellular CspA concentrations of up to 100 μM (6). CspA is an RNA chaperone that binds single-stranded nucleic acids, and destabilizes stem loop structures in nascent mRNA at low temperature, thus allowing transcription of downstream genes to continue under cold stress conditions

*To whom correspondence should be addressed. Tel: +33 4 57 42 85 62; Fax: +33 4 76 50 18 90; Email: bernhard.brutscher@ibs.fr

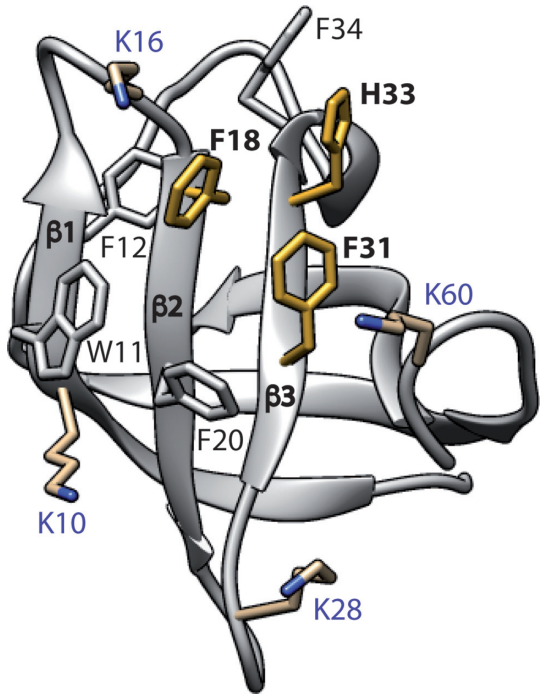

Figure 1. Ribbon representation of the *E. coli* CspA structure (PDB entry: 1MJC). The CspA orientation has been chosen so that the RNA interaction surface formed by strands β1–β3 is pointing towards the reader. Aromatic and positively charged Lysine side chains at the front side of the protein are also shown.

(7). In addition, enzymatic and chemical probing experiments have shown that the mRNA of CspA acts as a temperature sensor that switches between two conformations, with the low-temperature fold being more efficiently translated because of a more exposed ribosome binding site and a decreased susceptibility to degradation *in vivo* (8). At high concentration, CspA also down-regulates its own gene expression by binding to a RNA hairpin structure, the so-called cold-box, a conserved sequence motif among CSP genes located in the 5' untranslated region of the mRNA (9,10).

CSPs and CSDs share a common OB fold forming a five-stranded antiparallel β-barrel (Figure 1). High-resolution structures of CSPs have been determined by X-ray crystal diffraction (11,12) and solution NMR spectroscopy (13–16). These structures display a common nucleic-acid binding motif located on strands β2 and β3 that has been shown to bind to single-stranded DNA and RNA molecules with low sequence specificity and moderate binding affinity (K_d in the nanomolar to micromolar range). The binding surface comprises six aromatic residues and is flanked by several positively charged lysine residues (Figure 1). The available crystal structures of CSPs bound to single-stranded DNA (17,18) and RNA (19) oligonucleotides show that up to 5 nucleotide bases can be accommodated at the binding surface. It has also been reported that the three aromatic residues F18, F31 and H33 (CspA) are essential, and that mutation of one of these residues to leucine results in the complete loss of RNA chaperone activity and cold adaptation, while RNA binding seems not to be affected by these mutations (20,21).

Here, we report on the results of an NMR investigation aiming at an atomic-resolution description of the mode of action CspA employs to help RNA melting and refolding. To this end, we have set up an RNA duplex formation assay, and we have used a combination of real-time and steady-state multidimensional NMR approaches to obtain detailed information on the interaction of CspA with its RNA targets, and how the CspA-induced destabilization of RNA secondary structures affects the conformational dynamics and stability of the protein. In addition, we have used single-point mutants of CspA, as well as different types of peptides to investigate the influence of aromatic and positively charged amino-acid side chains on the RNA chaperone activity of the protein.

MATERIALS AND METHODS

RNA sample preparation

CB RNA samples with ^{13}C, ^{15}N labeled U and G nucleotides were produced by *in vitro* transcription with T7 RNA polymerase, using annealed full length double stranded oligonucleotides (Eurogentec) with the following sequences: 5'-*CTAATACGACTCACTATA*GGAGGTTT GGAAACAGACCATTA-3' and 5'-T(A$^{2'OMe}$)ATGGTC TGTTTCCAAACCTCC*TATAGTGAGTCGTATTAG-3'*. The modification of the penultimate nucleotide with a 2'-methoxy can significantly reduce $N + 1$ activity (data not shown) by the T7 RNA polymerase and increase the abundance of the desired RNA. In short, a mix was prepared containing the transcription buffer [40 mM Tris (pH 8), 5 mM DTT, 1 mM spermidine, 0.01% Triton X-100 and 80 mg/ ml PEG 8000], each rNTP at 4 mM, 20 mM MgCl2, 40 μg/ ml BSA, 1 U/ml of pyrophosphatase and the annealed template at 35 μg/ ml. ^{13}C, ^{15}N labeled rG and rU were purchased from CIL or Silantes. The reaction was started by addition of T7 RNA polymerase and allowed to proceed for 3 h at 37°C. Then, 50 units of RNase-free DNase were added, and the mix was incubated further for 30 min at 37°C. The reaction mixture was then diluted 10-fold in 20 mM Tris, 10 mM EDTA, and 8 M urea (pH 8.0) and loaded on a Q-Sepharose column equilibrated with the same buffer. The column was eluted with a gradient from 0 to 1 M NaCl in the same buffer. Fractions containing RNA, as determined by A260, were checked via denaturing 15% polyacrylamide gel electrophoresis. The fractions with the desired transcript were pooled, dialyzed three times against 200 volumes of H_2O, and lyophilized for storage. Before being used, the RNA samples were dissolved in the appropriate buffer and annealed by heating to 96°C for 5 min and flash cooling in an ice/water bath. RNA concentrations were estimated by measuring absorption at 260 nm in 8 M urea using the extinction coefficient of 40 μg/ml for 1 unit A260. In addition to the biochemically synthesized RNA samples, unlabeled and site-specific purine 8-^{13}C- or pyrimidine 6-^{13}C-labeled samples of CB and ACB were synthesized (22).

CspA expression and purification

His-tagged CspA in pETM11 plasmid was expressed in *E. coli* BL21 (DE3) in M9 medium containing 1 g/l of $^{15}NH_4Cl$ as the sole source of nitrogen. Cell cultures were grown at 37°C to an OD ~0.6, induced by addition of 0.4 mM IPTG and incubated at 30°C overnight. Harvested cell pellets were lysed by sonication in 30 ml of buffer A (10 mM BisTris, pH 7.0, 30 mM imidazole), 50 μg/ml DNAse I was added and the lysate was centrifuged. The soluble fraction was loaded onto a HisTrap FF 5 ml column (GE Healthcare) and washed with five column volumes of buffer A, followed by a wash of 10 column volumes of buffer B (10 mM BisTris, pH 7.0, 2 M NaCl, 50 mM imidazole) and another five column volumes of buffer A. Bound protein was eluted isocratically with 15 ml of buffer C (10 mM BisTris, pH 7.0, 300 mM imidazole, 1 mM EDTA). The protein sample was exchanged to buffer D (10 mM BisTris, pH 7.0, 1 mM EDTA) by concentration and dilution and concentrated to a final volume of 2 ml. At this point, 2-mercaptoethanol was added to a final concentration of 5 mM and the HisTag was cleaved off with 0.2 mg/ml of TEV protease at 4°C overnight. The sample was separated on a HiLoad 16/60 S30 column (GE Healthcare) equilibrated with the NMR buffer at a flow rate of 1 ml/min.

NMR spectroscopy

All experiments were performed on NMR spectrometers equipped with cryogenically cooled triple-resonance probes (HCN) and pulsed z-field gradients, either Agilent VNMRS 800 or Bruker Avance III HD 600, 700, 850 and 950 MHz instruments. The standard conditions for the NMR samples were 50 mM potassium phosphate, pH 6.5, 0.1 mM EDTA and 20°C.

For real-time NMR experiments, 300 to 350 μl buffer solution containing ACB and eventually the chaperone protein/peptides were filled in a 5 mm Shigemi tube (without plunger). To initiate the refolding reaction inside the NMR magnet, 100 μl of CB RNA dissolved in the same buffer were injected using a fast mixing device (23,24). The final RNA concentration was ~40 μM for the CB hairpin, and 50–70 μM for the ACB hairpin. Shimming on a reference sample was used to achieve good field homogeneity, sometimes helped by some additional shimming on the sample to be measured, before starting the NMR experiment, leading to a dead time of <1 min. The injection time was noted at the zero-time point of the refolding kinetics. A series of imino ^{1}H HADSOFAST spectra were recorded during the RNA refolding reaction with a time resolution of 10 s per experiment. Prior to Fourier transformation, the recorded data were combined using the appropriate Hadamard transformation to separate the NMR spectra of different species as explained in the text. Kinetic traces were then obtained for individual imino ^{1}H sites by extracting the signal intensities for individual peaks along the kinetic dimension. Subsequent data fitting was achieved using home-written Python scripts.

The imino ^{1}H frequencies of the two RNA hairpins and the hetero-duplex were sequentially assigned with the help of 2D BEST-optimized ^{1}H–^{1}H NOESY spectra recorded with a mixing time of 200 ms. BEST-optimization (25) allowed to enhance the overall sensitivity of the experiment by reducing the recycle delay to ~300 ms.

NMR assignment of the G and U nucleobase ^{1}H and ^{13}C frequencies in CB RNA was obtained through triple-resonance scalar correlation experiments (26,27). In the case of the chemically synthesized ACB RNA, the assignment was obtained by ^{13}C-edited NOESY experiments helped by ^{1}H–^{13}C correlation spectra recorded on ACB samples containing only a single ^{13}C label at the C_6 position of U5, U7 or U8.

For the chemical shift titration experiments, ^{15}N-labeled CspA and ^{13}C-labeled RNA (CB or ACB) were mixed at molar RNA/CspA ratios ranging from 0.25 to 4 with a constant protein concentration of $P_0 = 400$ μM, and put into separate sample tubes (either 3 mm or 1.7 mm diameter) for subsequent NMR measurements. To map the chemical shift changes induced by the intermolecular interaction both on the protein and on the RNA side, ^{1}H–^{15}N BEST-TROSY (28) and ^{1}H–^{13}C BEST-TROSY experiments were recorded on each sample. To determine the dissociation constant K_d of the interaction, the measured chemical shift changes for individual sites in the protein and the RNA were then fitted together to the following functions:

$$\Delta\delta_{CspA} = \frac{\Delta\delta_{max}}{2}\left\{(\mathrm{nx}+1+nK_d/P_0) - \sqrt{(\mathrm{nx}+1+nK_d/P_0)^2 - 4nx}\right\},$$

and

$$\Delta\delta_{RNA} = \frac{\Delta\delta_{max}}{2}\left\{(1/nx+1+K_d/xP_0) - \sqrt{(1/nx+1+K_d/xP_0)^2 - \frac{4}{nx}}\right\}$$

with $x = R_0/P_0$\$, and n an adjustable parameter that accounts for systematic errors in the measured RNA/protein concentration ratio.

The local and global rotational dynamics of CspA in the absence and presence of ACB RNA were studied by ^{15}N relaxation experiments. The overall correlation time, related to the size of the particle, was probed by means of a TRACT experiment (29) measuring the relaxation rate difference of the two doublet components of a ^{1}H-coupled ^{15}N in a series of 1D experiments. Fast local motions were probed by a heteronuclear NOE (HETNOE) experiment using a standard Bruker library sequence. Finally, exchange contributions to the transverse relaxation of ^{15}N (CspA) and ^{13}C (RNA) were probed by CPMG-type relaxation-dispersion experiments (30,31) using a relaxation delay of 60 ms (40 ms) for CspA (ACB), and CPMG frequencies ranging from 50 to 1000 Hz. Global data fitting to a 2-site exchange model was performed with the program CHEMEX (32).

Solvent hydrogen exchange rates of imino ^{1}H in CB and ACB RNA hairpins were measured using a 1D version of the CLEANEX-PM pulse sequence (33). For accurate quantification of exchange rates, four different types of experiments were performed: (i) exchange experiments for a series of exchange times τ_m; (ii) an experiment to measure the efficiency of the water saturation under steady state conditions, (iii) a reference experiment without the water saturation pulse and CLEANEX sequence. The latter experiment was recorded with an inter-scan delay of 10 s; and (iv) an experiment that measures the water ^{1}H longitudinal re-

laxation rate $R_1{}^W$. The exchange rates k_{ex}, and the apparent amide proton relaxation times $R_1{}^A$ are then obtained by a fit of the measured data to the following equation:

$$\frac{I^{ex}(t_m)}{I^{ref}} = \frac{k_{ex}/W^{sat}}{R_1^A + k_{ex}/W^{sat} - R_1^W}\left\{exp\left(-R_1^W t_m\right) - exp\left(\left(R_1^A + k_{ex}/W^{sat}\right)t_m\right)\right\}.$$

UV melting curves of RNA hairpins

Absorbance versus temperature profiles were recorded at 250 and 260 nm on a Cary-100 spectrophotometer equipped with a multiple cell holder and a Peltier temperature-control device. Data were collected for five heating cooling cycles at a rate of 0.7°C/min. Melting transitions were essentially the same with respect to the two different wavelengths and heating–cooling cycles. Melting point temperatures are reported as mean value of the five measurements. The RNA concentrations were 2 and 5 μM. At both concentrations, the same melting temperature (64.1°C CB hairpin, 78.1°C ACB hairpin) was determined indicative for a monomolecular hairpin fold. The buffer for the melting curve experiments was: 10 mM sodium phosphate, pH 7.0, 150 mM NaCl.

RESULTS

RNA folding kinetics and CspA chaperone activity

For the investigation of the chaperone activity of CspA (and other proteins), we have set up a simple RNA duplex formation assay involving two small complementary RNAs (~20 nucleotides), that both adopt stem–loop structures in solution. When mixed together they spontaneously refold to form the thermodynamically favored stable hetero-duplex fold (Figure 2A). The first RNA hairpin has been derived from the cold-box mRNA sequence of CspA, known to be a natural binding partner, by replacing the original loop nucleotides by a more stable GNRA tetra-loop, in order to avoid homo-dimerization of the RNA under our experimental conditions. Therefore, we will refer to this RNA hairpin as cold-box (CB) RNA, and in analogy the complementary RNA sequence is labeled anti-cold-box (ACB) RNA. The engineered hairpins differ in their nucleotide composition, base pairing, single-strand overhangs, and overall stability, and provide examples of potential mRNA structures that may be affected by CspA. The measured concentration-independent melting temperatures for the two RNA hairpins in the absence of CspA are 64.1°C for CB RNA and 78.1°C for ACB RNA (Supplementary Figure S1).

Real-time NMR spectroscopy has been chosen as experimental tool to obtain kinetic information for individual nucleotides during the RNA refolding event, and to identify potential intermediate-state conformations that become populated along the folding pathway(s). In order to initiate the refolding reaction, the two RNA hairpins, and eventually the chaperone protein, are mixed together inside the NMR magnet using a fast injection device (23,24). After injection, a series of one-dimensional (1D) or multi-dimensional (nD) NMR spectra is recorded during the

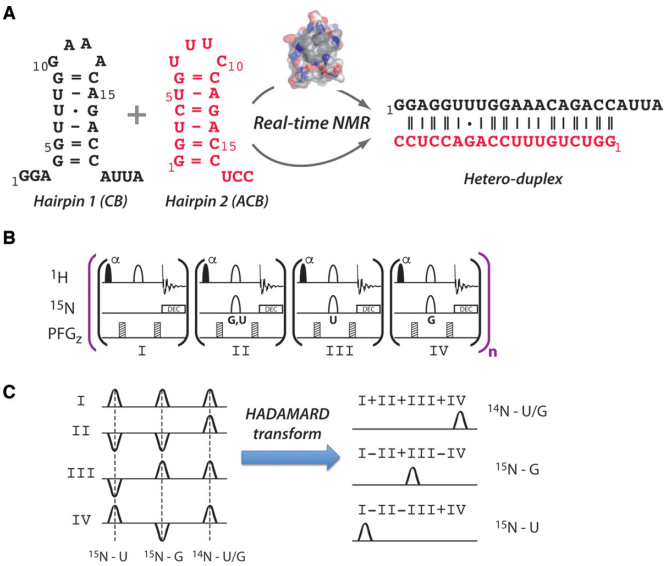

Figure 2. Experimental setup for probing RNA refolding and chaperone activity by time-resolved NMR spectroscopy. (**A**) RNA annealing assay consisting in two complementary RNA hairpins that spontaneously form a hetero-duplex conformation after mixing. (**B**) Imino-^{1}H HADSOFAST experiment for sample mixtures of unlabeled and ^{15}N-labeled RNA. The experiment is based on a SOFAST-HMQC (34,35) sequence with the first ^{1}H pulse applied with a PC9 shape (41) and a flip angle $\alpha = 120°$. All ^{1}H and ^{15}N 180° pulses are applied with REBURP shape (42). ^{1}H pulses are typically centered at 12.5 ppm covering a bandwidth of 5 ppm, while the ^{15}N pulse shape is changed between experiments to achieve HADAMARD sign encoding: (I) no ^{15}N pulse, ^{15}N pulse covering a band width of (II) 155 ± 15 ppm (U and G), (III) 161 ± 5 ppm (U only) and (IV) 146 ± 5 ppm (G only). The Imino-^{1}H HADSOFAST experiment is repeated n-times during the refolding process in an indirect dimension of a 2D NMR experiment. (**C**) Schematic drawing of the spectral deconvolution process required for obtaining NMR imino ^{1}H spectra of the three different species: ^{15}N-U, ^{15}N-G and ^{14}N-U/G.

course of the refolding reaction. A schematic drawing of the experimental setup is shown in the Supporting Information (Supplementary Figure S2). Imino protons provide convenient NMR probes for the study of RNA refolding kinetics as they give rise to a single NMR signal for each nucleotide involved in base-pairing interactions. Still, although we are dealing with small RNA molecules, the resolution in a 1D NMR spectrum is not sufficient for resolving all individual imino ^{1}H signals of the different RNA species occurring during the reaction. Also experimental sensitivity is a concern for real-time NMR experiments, especially when using low sample concentrations, as it is the case here (RNA concentration of ~60 μM). Therefore, in order to enhance the experimental sensitivity and apparent spectral resolution, we have used a combination of stable isotope (^{15}N) labeling of one of the RNAs by *in vitro* transcription, SOFAST NMR (34,35) and HADAMARD spectral encoding (36). The new imino-HADSOFAST experiment, depicted in Figure 2B consists in four repetitions of a basic pulse sequence differing in the ^{15}N 180° pulse applied during a transfer delay of length $1/(J_{NH})$, with J_{NH} the scalar coupling constant between the imino ^{1}H and ^{15}N. Changing the properties of this pulse results in a sign modulation of the observed imino ^{1}H signals depending on whether the attached nitrogen is ^{14}N or ^{15}N, and whether the corresponding RNA base is a

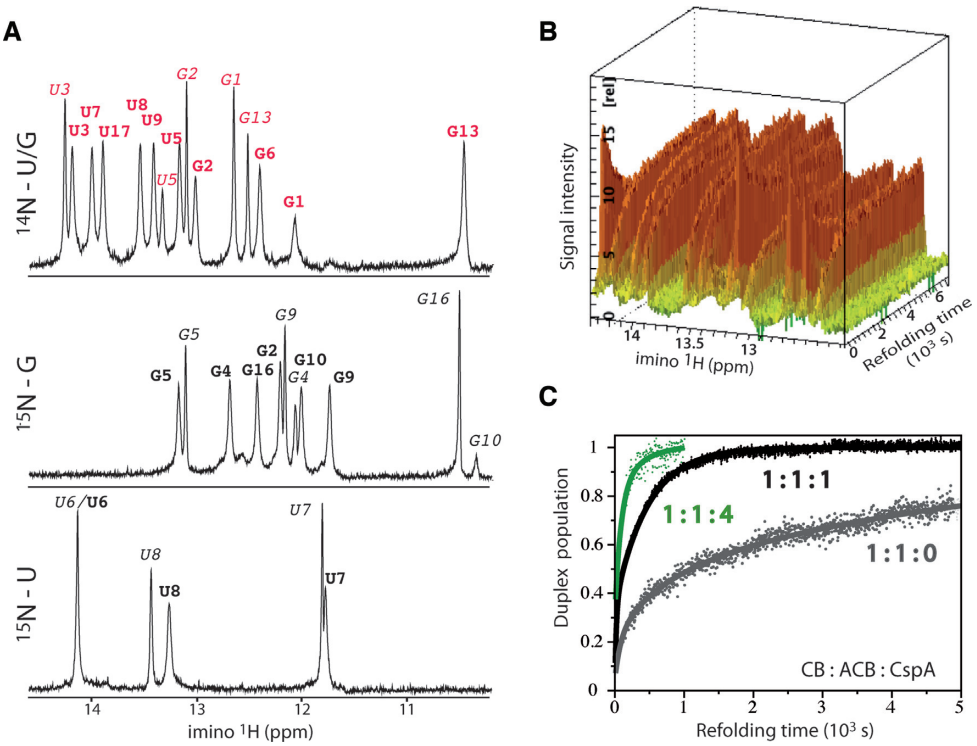

Figure 3. (**A**) 1D projections of an imino-^{1}H HADSOFAST experiment recorded at 950 MHz ^{1}H frequency during the RNA refolding assay depicted in Figure 2A, with ^{15}N labeled CB and unlabeled ACB. The RNA concentrations after the mixing are ~40 μM for CB and ~60 μM for ACB. Resonances from ACB are annotated in red color, while resonances from CB are annotated in black. Bold letters indicate an NMR signal from the hetero-duplex, while italic letters are used for the annotation of resonances from the RNA hairpins. (**B**) 2D real-time spectrum of ^{14}N-bound imino ^{1}H showing the ACB hairpin decay and duplex buildup (in presence of an equimolar amount of CspA) along the kinetic spectral dimension. Note that the ACB hairpin signals do not decay to zero because of an excess of ACB versus CB in the sample. (**C**) Normalized kinetics measured for RNA duplex formation in the absence of protein chaperone, in the presence of equimolar amounts of CspA, and a 4-fold excess of CspA. The displayed curves have been obtained by averaging over all individual traces from well-resolved imino ^{1}H of the RNA hetero-duplex.

purine (G) or pyrimidine (U). Spectral deconvolution by a so-called Hadamard transformation then results in the separation of the three different imino species (^{15}N-U, ^{15}N-G and ^{14}N-U/G), as illustrated in Figure 2C.

The result of real-time imino ^{1}H HADSOFAST experiments, performed after mixing the CB and ACB hairpin, with or without CspA, at 20°C using a fast injection device is shown in Figure 3. The repetition of the basic experiment along an additional kinetic dimension results in a 2D NMR spectrum with one frequency (imino ^{1}H chemical shift) and one time-axis (Figure 3B) for each of the three species (^{15}N-U, ^{15}N-G and ^{14}N-U/G). The time resolution of the kinetics is 10 s. As can be appreciated from the 1D projections taken along the kinetic dimension (Figure 3A) of the imino ^{1}H HADSOFAST experiment, all imino ^{1}H sites in the three RNA molecules are spectrally resolved, with the exception of U6 that resonates at identical NMR frequency in the CB hairpin and in the hetero-duplex. Complete resonance assignment of the observed imino ^{1}H signals has been obtained by means of 2D ^{1}H–^{1}H BEST-type NOESY experiments recorded on NMR samples of isolated RNA hairpins or the hetero-duplex. These data also validate the secondary structures of the RNAs as depicted in Figure 2A. In the absence of CspA, the two complementary RNA molecules undergo a spontaneous, but slow transition from the monomeric hairpin structure to the energetically favored hetero-dimer with a kinetic half-time constant of ~ 4 h. No NMR signal other than those expected for the adduct and product RNAs of the refolding reaction could be detected in the real-time NMR experiment, indicating that no differently structured and highly populated long-lived state is present during the refolding kinetics. Adding the kinetic traces (signal intensity as a function of refolding time) obtained for individual sites in the same RNA species increases the apparent signal-to-noise ratio of the data, and provides a measure of the average kinetics experienced by each of the RNAs (Figure 3C). The observed average RNA refolding kinetics, both in the absence and presence of the chaperone protein, is reasonably well described by a bi-exponential function with a fast and a slow kinetic phase. Non-linear data fitting then yields unfolding and folding rates, as well as amplitudes for the two kinetic phases that are summarized in Table 1. In the presence of an equimolar amount of CspA protein, the reaction is accelerated by one order of magnitude, while a four-times higher CspA:RNA ratio results in a 50-fold acceleration of hetero-duplex formation.

NMR spectroscopy has the resolving power to extract kinetic information for each individual, well-resolved imino ^{1}H site in the three RNA molecules (Supplementary Figure S3), providing important information on the folding pathways, as well as the chronology of the formation and de-

Table 1. RNA refolding kinetics measured by real-time NMR in the absence or presence of a chaperone protein or peptide

	$t_{1/2}$ (s)	λ	k_{fast} (10^{-3} s^{-1})	A_{slow}	k^{f}_{slow} (10^{-5} s^{-1})	$k^{uf,\,CB}_{slow}$ (10^{-5} s^{-1})	$k^{uf,\,ACB}_{slow}$ (10^{-5} s^{-1})
RNA alone	14 980	—	1.2 ± 0.1	0.68 ± 0.01	3.0 ± 0.1	4.3 ± 0.1	2.8 ± 0.2
FFF	7580	2.0	1.4 ± 0.1	0.66 ± 0.01	4.0 ± 0.1	4.9 ± 0.1	4.0 ± 0.2
CspA-F18I	6350	2.4	1.8 ± 0.1	0.68 ± 0.01	4.9 ±0.1	6.2 ± 0.1	5.3 ± 0.1
CspA-F12I	2700	5.5	3.5 ± 0.1	0.62 ± 0.01	7.5 ± 0.1	8.6 ± 0.1	7.2 ± 0.1
CspA-WT-1	1230	12.2	4.1 ± 0.1	0.64 ± 0.03	20.2 ± 0.1	31.6 ± 0.3	20 to 33
CspA-WT-2	300	50	12.8 ± 4.7	0.60 ± 0.03	70.5 ± 5.4	48.0 ± 3.6	n.d.
KKK	6820	2.2	1.3 ± 0.1	0.64 ± 0.1	4.5 ± 0.2	5.9 ± 0.3	3.1 ± 0.2
PV Core	3570	4.2	1.7 ± 0.2	0.68 ± 0.01	9.2 ± 0.2	8.5 ± 0.1	7.6 ± 0.2
poly-K	760	19.7	3.0 ± 0.4	0.45 ± 0.02	15.8 ± 1.3	20.8	n.d.

For non-linear data fitting, the kinetic profiles obtained from individual imino protons of the same RNA species (CB, ACB, duplex) were added. The following bi-exponential fit functions were used for a global fit: $I^{CB,ACB}(t) = B\{A_{slow}\exp(-k^{uf}_{slow}\,t) + (1 - A_{slow})\exp(-k_{fast}\,t)\} + C$ (CB and ACB decay), and $I^{duplex}(t) = D\{A_{slow}(1 - exp(-k^{f}_{slow}\,t)) + (1 - A_{slow})(1 - exp(-k_{fast}\,t))\}$ (duplex build up). Note that the same 'fast' rate constant was assumed for the unfolding and folding processes, while different 'slow' rates were fitted for the CB and ACB unfolding, and the hetero-duplex formation. Error estimations were obtained from a covariance matrix analysis. The enhancement factor λ was computed as $\lambda = t_{1/2}(\mathrm{RNA})/t_{1/2}(\mathrm{RNA + chaperone})$.

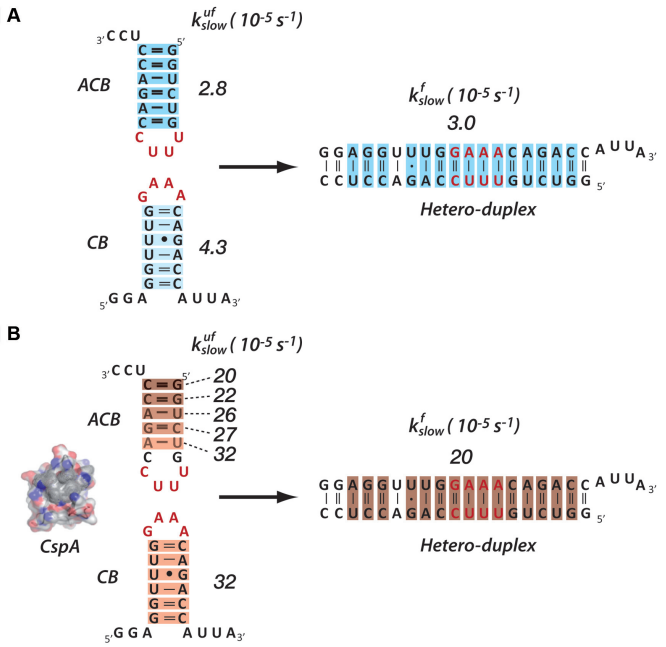

Figure 4. RNA hairpin unfolding and hetero-duplex folding rates, measured for the slow kinetic phase for individual base pair hydrogen bonds, are given and color-coded on the RNA structures in the absence (**A**) and presence (**B**) of CspA.

formation of hydrogen bonds as experienced by the imino protons of different RNA residues. For RNA duplex formation and CB RNA decay, both in the presence and absence of CspA, our data indicate that the local differences are negligible with respect to the experimental uncertainty. For the decay of the ACB RNA signals, however, the situation is different. While in the absence of chaperone protein, the kinetics for individual imino protons are very similar (Figure 4A), in the presence of CspA the kinetic rates of the slow unfolding process show a gradual increase from the stem end (G1) toward the loop (U5) with a 65% difference in the unfolding rate between the two stem ends (Figure 4B). This finding indicates that the melting of the ACB hairpin in the presence of CspA is a step-wise process, where CspA acts as a molecular zipper proceeding from the stem loop to the stem ends.

Our kinetic data allow extracting meaningful unfolding rates only for the slow phase of the observed CB and ACB decay curves (Table 1). No reliable information was obtained for the fast kinetic phase, mainly because the signal intensity at time $t = 0$ is not known due to the experimental dead time of ∼30 s. The slow unfolding and folding pathways account for ∼65% of RNA duplex formation, both in the presence and absence of chaperone protein. In agreement with the measured thermal stability of the two RNA hairpins (Supplementary Figure S1), we observe slightly higher unfolding rates for the CB RNA than for the ACB RNA (Figure 4A). CspA mainly accelerates the slow phase of the reaction by destabilizing the ACB hydrogen bonds close to the loop (Figure 4B), resulting in an overall increase of the unfolding rates for both hairpins, as well as a gradual increase within the ACB double-stranded segment. Interestingly, the kinetic rate for duplex formation is identical (within the experimental error) to the slowest unfolding rate observed for the different hydrogen bonds in the RNA hairpins, indicating that the formation of an extended stable RNA duplex requires the complete melting of both RNA hairpins. This conclusion holds true whether the chaperone protein CspA is present or not.

CspA–RNA binding and RNA hairpin destabilization

In order to further characterize the interaction of CspA with the individual RNA hairpins used in our refolding assay (Figure 2A), we have performed a number of additional NMR experiments under equilibrium (steady-state) conditions at 20°C. On the RNA side, imino ^{1}H, $^{13}C_6$ (U) and $^{13}C_8$ (G) base nuclei serve as local reporters of local changes induced by CspA binding. The effects observed in the NMR spectra of the two RNA hairpins (Figure 5) when adding equimolar amounts of CspA can be classified into three categories: sites without a significant spectral change, sites experiencing chemical shift changes, and sites characterized by extensive line broadening. The line broadening can be ascribed either to the presence of exchange dynamics on the micro- to milliseconds time scale or, in the case of imino protons, to the destabilization of the hydrogen-bonded base pairing. Additional quantitative information

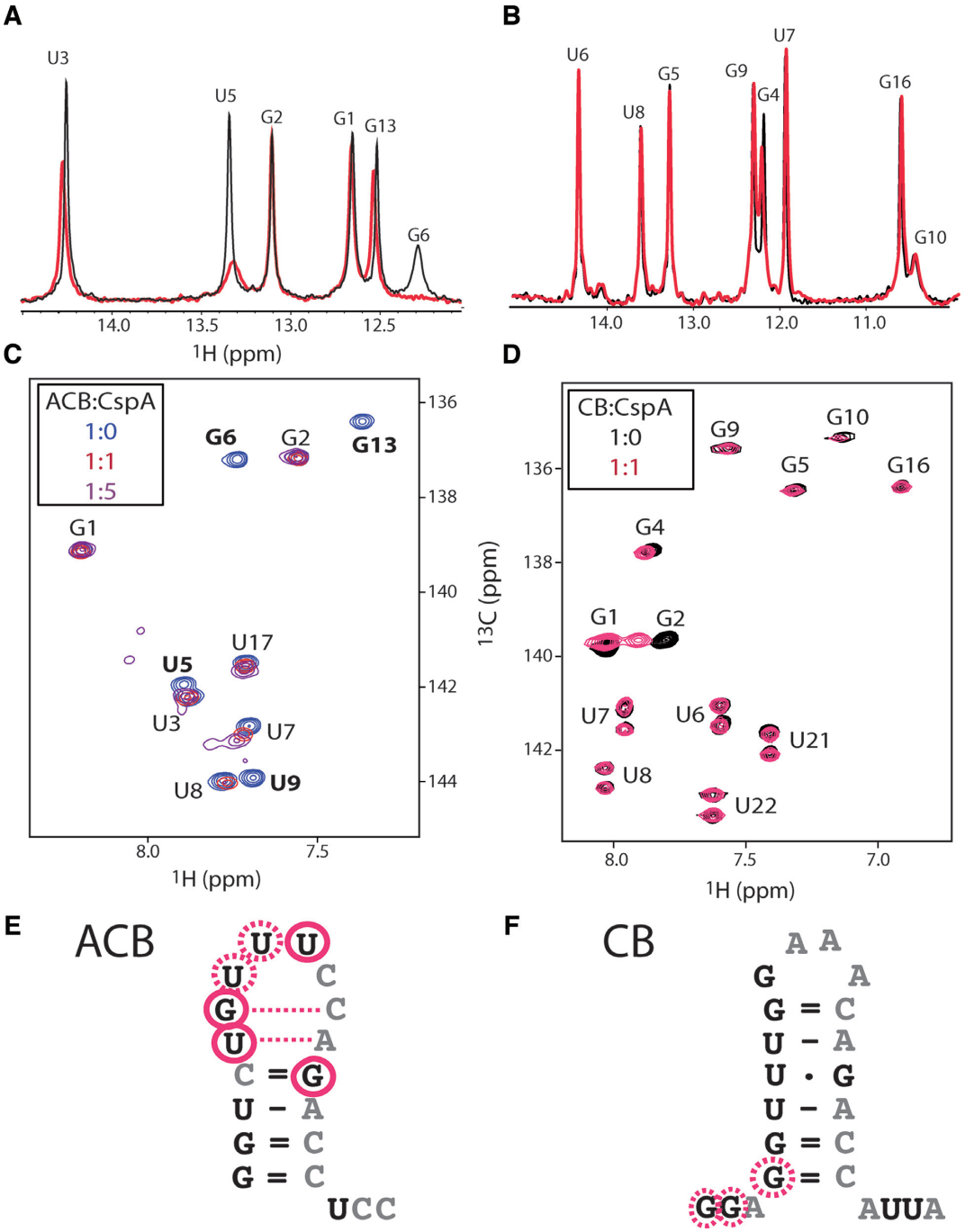

Figure 5. Imino ^{1}H NMR spectra of ACB (**A**) and CB (**B**) RNA hairpins in the absence (black) and presence (red) of an equimolar amount of CspA. The base regions of 2D ^{1}H–^{13}C correlation spectra are plotted in (**C**) for ACB and in (**D**) for CB. The observed spectral changes are summarized in (**E**) and (**F**) on the secondary structure of the two RNA hairpins. Closed circles indicate RNA bases with ^{1}H–^{13}C cross peaks that show significant line broadening in the presence of CspA, while dashed circles are used for RNA bases experiencing NMR chemical shift changes. Also the weakening of particular hydrogen bonds as inferred from the imino ^{1}H spectra and the measured hydrogen exchange rates is highlighted by red color.

on the hydrogen bond strengths in the RNA stems was obtained from hydrogen-solvent exchange measurements using the CLEANEX-PM experiment (33). The measured exchange rates with and without CspA are summarized in Table 2. The conclusions from these NMR measurements are summarized in Figure 5E and F for ACB and CB, respectively. CspA interacts with ACB mainly by binding to nucleotides of the stem loop. This interaction results in a destabilization of the two upper H-bonds in the stem (G6-C11 and U5-A12), as evidenced by significant line broadening of the corresponding imino ^{1}H resonances, as well as a significant increase of the observed hydrogen exchange rates. The CspA interaction with CB only affects the single-stranded 5' overhang (GGA) of the hairpin. The CspA in-

Table 2. Hydrogen exchange rates k_{ex} measured for imino protons involved in base-pairing interactions in CB and ACB RNA in the absence and presence of the chaperone protein CspA at equimolar concentration

CB	RNA alone k_{ex} (s^{-1})	With CspA k_{ex} (s^{-1})	ACB	RNA alone k_{ex} (s^{-1})	With CspA k_{ex} (s^{-1})
G4-C19	8.2 ± 0.4	13.1 ± 0.7	**G1**-C16	9.2 ± 0.3	11.1 ± 0.3
G5-C18	0.4 ± 0.2	1.6 ± 0.3	**G2**-C15	0.4 ± 0.2	0.3 ± 0.1
U6-A17	3.1 ± 0.2	5.4 ± 0.3	**U3**-A14	1.0 ± 0.2	0.5 ± 0.2
U7-G16	4.9 ± 0.3	8.1 ± 0.3	C4-**G13**	0.8 ± 0.3	0.3 ± 0.2
U7-**G16**	6.1 ± 0.6	10.8 ± 1.2	**U5**-A12	3.9 ± 0.2	24.8 ± 2.9
U8-A15	13.8 ± 0.6	18.7 ± 0.7	**G6**-C11	44.1 ± 1.5	>150 s^{-1}
G9-C14	3.2 ± 0.3	7.2 ± 0.4			
G10-??	95 ± 4.8	101.5 ± 12.7			

duced chemical shift changes observed for nucleotides G1, G2 and G4 are small, and no line broadening is observed for the base ^{13}C, indicative of a fast exchanging complex, and thus weak binding affinity. The imino ^{1}H spectrum remains unchanged, except for the first nucleotide at the bottom of the stem (G4) that becomes slightly line-broadened, in agreement with the finding that this base pair is closest to the CspA binding site. No binding to the GAAA loop or the single stranded 3'-terminus (AUUA) is observed. The measured hydrogen exchange rates show a slight destabilization of hydrogen bonds in the entire stem upon interaction with CspA.

In view of these results, we have decided to look in more detail at the CspA-ACB interaction that has a higher binding affinity compared to CspA-CB, and leads to a more pronounced destabilization of the base pairing in the hairpin stem. CspA ^{1}H–^{15}N correlation spectra recorded during a titration experiment at 20°C, where the CspA concentration was kept constant (400 μM) and the ACB concentration was varied from 0 to 1.6 mM, are shown in Figure 6A. Similar to the effects observed for the CB RNA, the presence of ACB results in line broadening of a large number of protein amide resonances. Localizing these line-broadening effects on the ribbon structure of CspA (Figure 6C) clearly identifies the surface region comprising β-strands 1, 2 and 3 as the binding side for the RNA, very similar to what has been observed for CspA-binding to other RNA sequences. A number of amide sites close to this primary contact site are in fast exchange, and show linear chemical shift changes during the titration. Our findings that the presence of CspA mainly affects a few loop nucleotides of the RNA hairpin that interact with the well-known RNA-binding surface of CspA, point toward a simple 1:1 interaction model. The rotational diffusion properties of the CspA–ACB complex as probed by a TRACT (29) experiment (Supplementary Figure S4) are also in good qualitative agreement with a 1:1 binding stoichiometry. Allowing for some readjustment of the relative RNA and protein concentrations, model fitting of the chemical shift variations observed for amide sites in CspA, and base ^{1}H and ^{13}C in ACB yields a dissociation constant $K_d = 12 \pm 2$ μM (Figure 6B) for the interaction between CspA and the ACB RNA hairpin. The exchange rate between free and bound CspA has been determined from CPMG relaxation–dispersion (RD) experiments (Supplementary Figure S5) as $k_{ex} = 550 \pm 30$ s^{-1}. Only nuclear sites with flat dispersion profiles in the free form have been used for the analysis. The minor state population, corresponding to free CspA, under the chosen experimental conditions (CspA:ACB = 1:2) has been estimated from the CS titration data, $P_{CspA,free} = 5.4 \pm 0.8\%$. Exchange contributions to the ^{13}C transverse relaxation rates are also detected for two nucleotides, U7 and U8, in the ACB hairpin loop. The ^{13}C relaxation-dispersion profiles measured for these two nucleotides (Supplementary Figure S6) agree well with the binding kinetics determined from the CspA chemical shift and CPMG data: the RNA exchanging between a free and CspA-bound state at a rate of 550 s^{-1}, and both states populated at ~50% under the conditions (protein and RNA concentration) used for the experiments (Figure 6B).

RNA binding-induced conformational stabilization of CspA

As reported previously (13), conformational dynamics at the micro- to millisecond time scale are observed at 20°C for many amide sites in the β-sheet structure of free CspA at 20°C. These conformational dynamics are particularly pronounced in β-strands 1, 2 and 3, that form the RNA binding interface (Figure 6C). It is well known that conformational flexibility plays a key role in molecular recognition, and it may be also important for the protein's RNA chaperone activity. In order to address this hypothesis, we have compared ^{15}N relaxation data, and in particular CPMG-RD data, measured on free and ACB-bound CspA. Unfortunately, for many of the amide sites undergoing slow conformational exchange in the free form, no CPMG-RD data were obtained in the complex due to extensive line broadening, or the dispersion curves were dominated by the exchange dynamics between free and RNA-bound CspA. Still, a few residues (I21, E56, V67) could be identified for which the conformational dynamics observed in the free form is quenched in the RNA-bound form, or shifted outside the millisecond time scale.

Additional information on the stabilization of the CspA fold upon RNA binding was obtained from NMR data recorded at a higher sample temperature of 45°C. At this temperature, CspA, with a reported melting temperature of $T_M = 60$°C (11), starts to unfold, while ACB still forms a stable RNA hairpin ($T_M = 78$°C). A consequence of the increased temperature is a shift of the exchange rate between free and ACB-bound CspA from $k_{ex} \approx 550$ s^{-1} to $k_{ex} \approx 1000$ s^{-1}, as estimated from the largest chemical shift changes still observable. Under these 'fast exchange' conditions, most amide sites show linear shifts in the NMR spectra when adding increasing amounts of ACB (Figure 7A and B), and line broadening is reduced to a few CspA residues with the largest chemical shift changes between the free and bound forms. Fitting these titration data yields an apparent K_d of

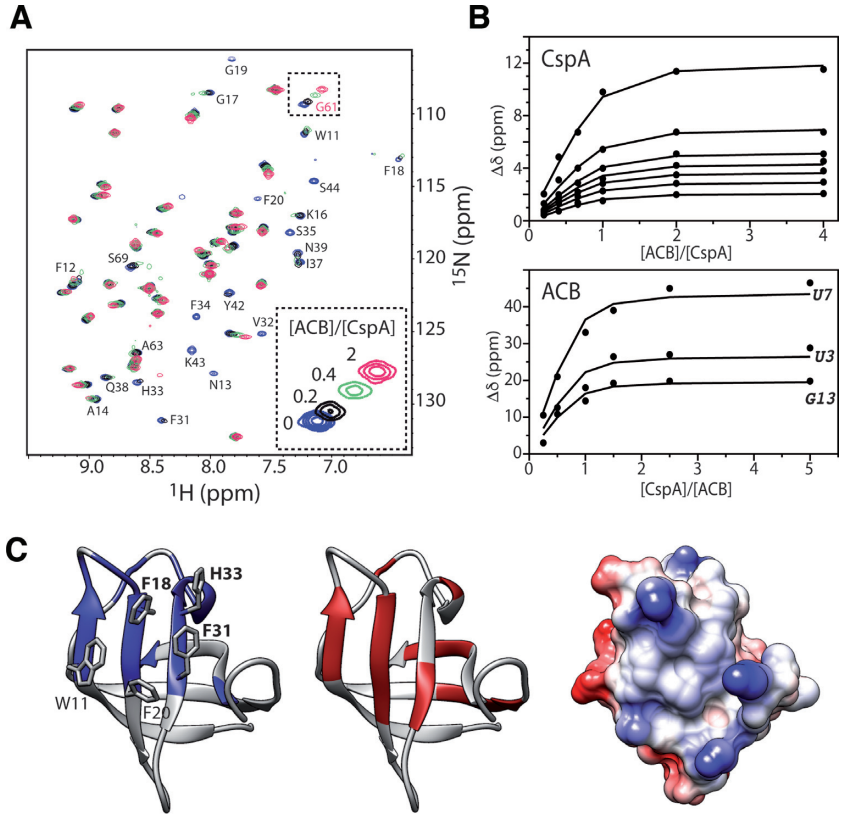

Figure 6. NMR characterization of the CspA–ACB interaction at 20°C. ^{1}H–^{15}N BEST-TROSY (28) spectra recorded for CspA in the presence of different amounts of RNA are superposed and color-coded in (**A**). A large number of amide sites show extensive line broadening in the presence of CspA, while others undergo peak shifts, indicating a rather fast exchange process between the free and the bound form. (**B**) Fitting the measured chemical shift data for CspA and ACB together, assuming a CspA:ACB stoichiometry of 1:1, yields an apparent K_d of 12 ± 2 μM. (**C**) Residues with extensive line broadening upon CspA binding (11–14, 16–20, 31–39, 42–44, 63, 69) are highlighted in blue on the ribbon structure of CspA (left panel), while residues undergoing conformational exchange (11–13, 18–21, 30–31, 35, 42–43, 53–56, 66–68) as probed by relaxation-dispersion NMR are shown in red (central panel). In addition, the electrostatic surface potential of CspA is plotted (right panel) using the same orientation of the molecule.

50 ± 3 μM (Supplementary Figure S7). The unfolding dynamics of free CspA induce conformational exchange contributions to the transverse ^{15}N relaxation rates throughout the protein (Figure 7C). At 45°C, ^{15}N relaxation parameters were obtained for a large number of amide sites in the complex. Most interestingly, we observe that the unfolding dynamics are quenched upon RNA binding (Figure 7C); only some residues at the binding interface still experience conformational-exchange induced line broadening that can be ascribed to the exchange of the complex with ∼18% of free CspA under these experimental conditions. Fast timescale dynamics (ps–ns), as probed by heteronuclear NOEs, are mainly detected in some loop regions of CspA and are not significantly influenced by RNA binding (Figure 7D). Our results indicate that RNA-binding results in a stabilization of the CspA fold.

Influence of structure, key aromatic residues and positive charges on RNA chaperone activity

As shown in Figure 6C, the RNA binding site of CspA comprises five aromatic residues, three of which (F18, F31 and H33) have been reported to be essential for RNA chaperone activity (21). The interaction surface is positively charged due to the presence of a number of lysine residues, thus favoring recognition and interaction of the binding interface with the negatively charged phosphodiester backbone of RNAs. In order to investigate further the importance of these key aromatic residues and their relative conformation for RNA annealing, we have prepared two CspA single-point mutants: F18I, where one of the essential residues for chaperone activity has been replaced by isoleucine, and F12I, where an aromatic side chain that is not directly involved in RNA binding has been replaced by an aliphatic side chain to destabilize the protein fold. The NMR spectra of the two CspA mutants are shown in Supplementary Figure S8. As expected, the replacement of the aromatic side chain on the protein surface (CspA-F18I) does not perturb the protein fold, and spectral changes are limited to residues spatially close to the mutated site. The F12I mutation, however, results in a ^{1}H–^{15}N correlation spectrum of poor overall quality with a heterogeneous peak intensity distribution. This spectrum is indicative of a molten globular state, i.e. a protein with a high degree of conformational flexibility, or a protein in exchange between folded and unfolded conformations.

We have tested the chaperone activity of these two CspA mutants by real-time NMR using the RNA annealing assay and NMR methodology described above (Figure 2). In

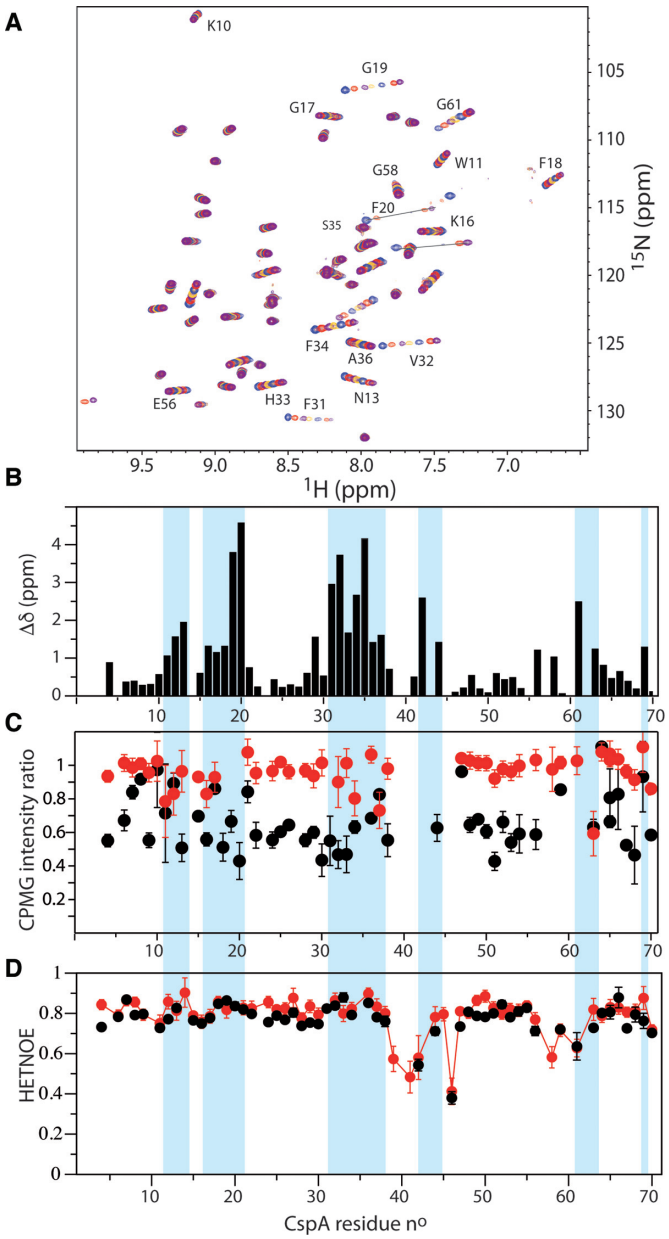

Figure 7. NMR characterization of the CspA–ACB interaction at 45°C. (**A**) Superposition of NMR ^{1}H–^{15}N correlation spectra recorded for different CspA–ACB mixtures. (**B**) Chemical shift differences observed between free and bound CspA. The plotted values have been calculated as $\Delta\delta = \sqrt{(10\Delta\delta_H)^2 + (\Delta\delta_N)^2}$. The peptide regions with the largest chemical shift changes ($\Delta\delta > 1$) are highlighted in light blue. As expected, this RNA binding site is identical to the results obtained at 20°C (Figure 6C). (**C**) Intensity ratios measured for individual ^{1}H–^{15}N correlation peaks from two CPMG-RD spectra using CPMG frequencies of 33 and 1000 s^{-1}, respectively. CPMG intensity ratios of free CspA are plotted in black, while those of CspA in complex with ACB RNA are shown in red. (**D**) {^{1}H}–^{15}N heteronuclear NOE (HETNOE) data measured for free CspA (black) and CspA in complex with ACB RNA (red).

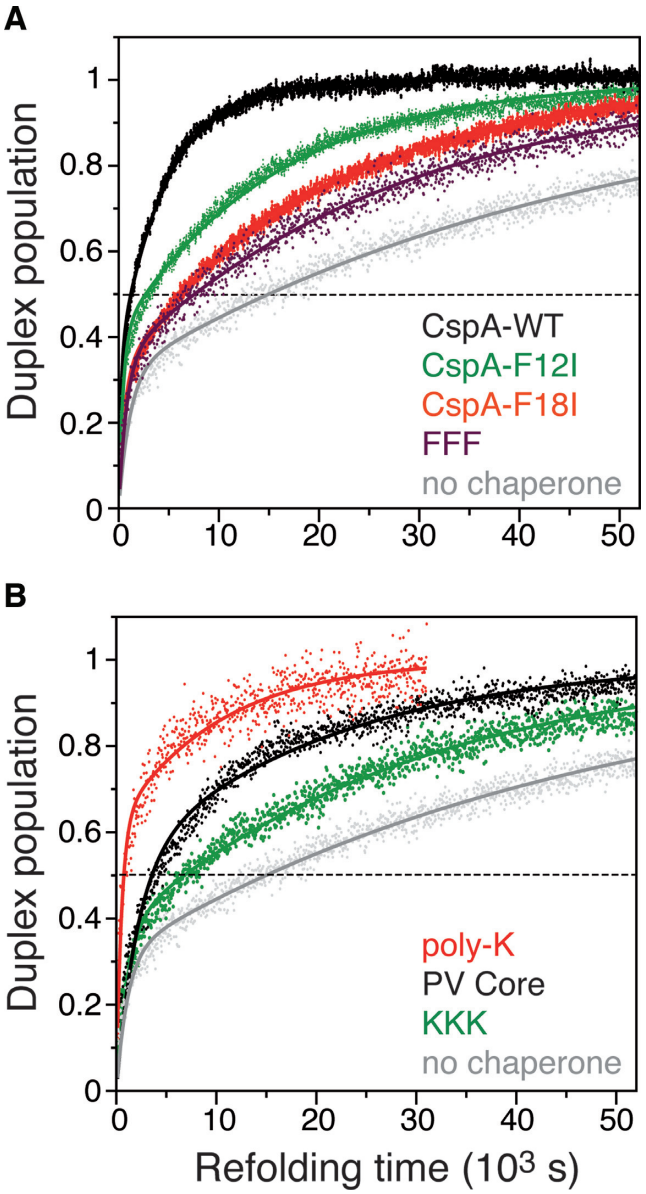

Figure 8. Normalized real-time NMR kinetics measured for RNA duplex formation in the presence of (**A**) CspA-WT (black), CspA-F12I (green), CspA-F18I (red), F-F-F peptide (purple), and (**B**) PV core (black), triple-K (green) and poly-K (red). In addition, the folding kinetics in the absence of any protein or peptide is shown in gray in both graphs. The displayed data points have been obtained by averaging over all individual traces from well-resolved imino ^{1}H of the RNA hetero-duplex, and the lines represent the results of a data fit to a bi-exponential model.

addition, we have also investigated the effect of a simple phenylalanine tri-peptide (FFF) on the RNA refolding kinetics. The measured kinetic traces of RNA duplex formation in the presence of the different proteins/peptides are plotted in Figure 8A, and the results of data fitting to a bi-exponential model are given in Table 1. Interestingly, both CspA mutants as well as the FFF peptide show some RNA chaperone activity, although reduced with respect to WT CspA. On the one hand, removing a single aromatic side chain (F18) from the interaction surface of CspA results in an about 6-fold reduction in RNA annealing efficiency, very similar to what is observed for the FFF tripeptide. However, RNA annealing is still about a factor of 2 faster than in the absence of any protein or peptide. On the other hand, destabilizing the protein fold by the F12I mutation still ac-

celerates the RNA refolding by a factor of 5 to 6, which is only two-times less efficient than WT CspA. We may speculate that the observed high level of RNA chaperone activity comes from the fact that native-like conformations are still transiently sampled to high levels in this dynamic CspA mutant. In summary, our results demonstrate that aromatic peptide side chains have an effect on the annealing of RNA secondary structure, most likely by destabilizing base pairing and stacking interactions. This chaperone activity seems to be enhanced by the cooperative action of several aromatic side chains with a well-defined spatial arrangement, as found on the surface of CspA.

The RNA-binding interface of CspA also contains a number of positively charge lysine residues (Figure 1). In order to investigate the effect of positive charges on the RNA refolding kinetics, we adopted a slightly different strategy. We have compared the chaperone activity of CspA with a range of positively charged peptides: (i) a tri-lysine (KKK) peptide, (ii) a mixture of poly-lysine peptides (poly-K) of different lengths (17–67 residues) and (iii) the core protein of Pestivirus (PV), an intrinsically disordered protein that has been shown to possess RNA chaperone activity (37). 27% of the PV core residues are positively charged R or K amino acids. The primary sequence of PV core, as well as a ^{1}H–^{15}N correlation spectrum, and a plot of the secondary structural propensities as determined by NMR chemical shifts are shown in Supplementary Figure S9. Again, real time NMR measurements probing the RNA refolding kinetics have been performed in the presence of the different peptides, and the results are plotted in Figure 8B. All positively charged peptides accelerate RNA duplex formation by a factor of ~2 for KKK, ~4 for PV core, and ~20 for poly-K. These results suggest that the number, length and potentially distribution of positively charged peptide stretches are the main determinants for the charge-induced RNA chaperone activity.

DISCUSSION

RNA annealing and refolding: from kinetic data to a mechanistic model

In contrast to most alternative biophysical or biochemical techniques, time-resolved imino ^{1}H NMR spectroscopy allowed us to measure kinetic profiles of hydrogen bond formation and disruption simultaneously for all RNA species and individual nucleotides in an RNA annealing assay consisting of two complementary RNA hairpins that spontaneously refold to form a thermodynamically more stable hetero-duplex. In the presence of CspA, this has allowed us to detect the unzippering of hydrogen bonds in one of the RNA hairpin stems as a gradual increase in the measured unfolding rates. Our finding implies the presence of partially folded intermediate states of this RNA hairpin (ACB) as a consequence of the chaperone's RNA melting activity. These short-lived states, however, do not give rise to a specific NMR signature (set of imino ^{1}H resonances) distinguishable from the fully folded RNA hairpin structure. All observed kinetics are (at least) bi-exponential, indicating the presence of (at least) two parallel folding pathways. RNA annealing and duplex formation requires the presence of short complementary single-stranded RNA stretches lacking any persistent intra-molecular base pairing that can serve as a starting site for duplex formation. Subsequently, to push forward the hetero-duplex fold formation, base pair interactions in the RNA hairpins need to be disrupted. Breaking the base-pair interactions of the most stable RNA hairpin therefore presents the rate-limiting step of the duplex formation reaction. A general folding model is shown in Figure 9A. In a first step of this model, the two hairpins form various types of encounter complexes with only weak and transient interactions between them, making the NMR detection of these states impossible. Our NMR data, however, do not provide any evidence which type of encounter states is responsible for the observed fast and slow kinetic phases. The on-rate (k_{on}) of this second-order bimolecular reaction is supposed to be diffusion limited, while the off-rate (k_{off}) depends on the strength and nature of the intermolecular interactions, as well as the ability to proceed further to the formation of transition states that lead to the disruption of hydrogen bonds in the RNA hairpins. Finally, once the two RNA hairpins are sufficiently unfolded, duplex formation occurs at a very fast rate. The encounter complexes are divided into two classes to account for the observed bi-exponential kinetics. The first class (EC-1) is characterized by large k_{off} rates, and thus short lifetimes and low overall population, but with a high propensity to proceed with transition state and duplex formation. This pathway accounts for the fast kinetic phase. The second pathway, leading to slow unfolding and folding rates, is described by encounter states (EC-2) that are longer lived, but adopt a more unfavorable conformation for hydrogen-bond breaking and duplex formation.

CspA interaction with RNA hairpin structures

So far, only interaction studies between cold-shock domains and single-stranded RNA or DNA have been reported in the literature. It has been shown that Csps bind preferentially to single-stranded RNA (ssRNA) regions of at least four nucleotides in length (38), with increasing affinity for longer sequences of six or seven nucleotides, and a preference for pyrimidine-rich stretches (19). Here, we have characterized for the first time the binding of CspA to two small RNA hairpins. Although this was not a major objective of this study, our NMR data provide some insight into the requirements for CspA binding to RNA hairpin structures. CspA can interact with RNA hairpins either via the single-stranded overhangs or the hairpin loop. The ACB hairpin loop provides the most suitable target for CspA binding, as it is rich in pyrimidines (U-U-U-C) and not significantly stabilized by base pairing interactions. The situation is different for the stabilized purine-rich GNRA tetraloop (G-A-A-A) of CB RNA that does not show any interaction with CspA. Somewhat surprisingly, we also observed weak CspA interaction with the three-nucleotide G-G-A overhang at the 5'-end of CB, while no interaction is observed with either the longer A-U-U-A 3'-end of CB, or the U-C-C overhang of ACB. We may therefore argue that the conclusions drawn from interaction studies of CspA with 6- or 7-nucleotide ssRNA stretches do not hold for weak, sub-optimal binding to shorter RNA sequences. Not surprisingly the binding affinities measured for the CspA–

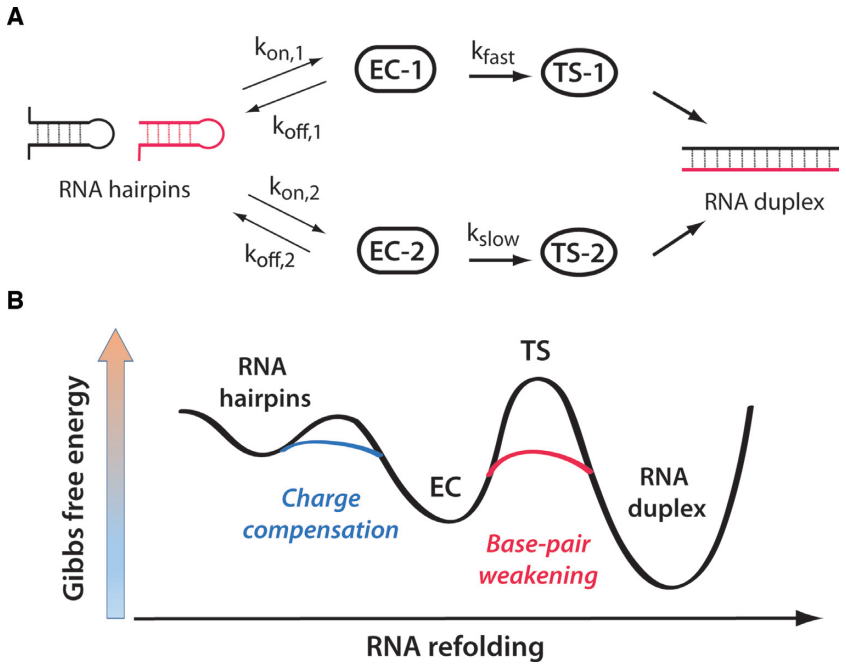

Figure 9. Possible (parallel) duplex formation models. (**A**) Initially, the two strands can form structurally different encounter complexes (EC-1 and EC-2) with only weak and transient interactions. Then, respective transition states are formed with distinct fast (TS-1) and slow (TS-2) kinetic signatures. Finally, the folding reaction proceeds via disruption of the hairpin base pair interactions, followed by the formation of new intermolecular base pairs leading to the final hetero-dimer RNA. (**B**) Gibbs-free energy profile corresponding to the folding model presented in (A). Charge compensation reduces the activation energy for encounter state formation, while chaperone-induced base-pair opening lowers the free energy of the transition states.

ACB hairpin interaction are one to two orders of magnitude lower than reported for *B. subtilis* CspB binding to various ssRNA sequences (19). The temperature dependence of the apparent dissociation constants of the CspA-ACB interaction, as determined by NMR titration experiments, also allows some estimation of the enthalpic and entropic contributions to the binding free energy. In particular, the entropy change is found to be only $\Delta S = -60 \pm 20$ J/mol K, compared to literature values (19) for cold shock proteins binding to single-stranded RNA or DNA of $\Delta S = -300$ to -360 J/mol K. This reduced entropic penalty is most likely explained by the more rigid stem–loop structure of the ACB RNA compared to single-stranded nucleic acids.

A rather general aspect of cold shock domain proteins seems to be the loss in global entropy upon RNA or DNA binding. For *E. coli* CspA, we have demonstrated here that under temperature conditions (45°C) where part of the protein is unfolded, binding to an RNA hairpin shifts the population equilibrium toward the folded state. Similar observations have been made for *B. subtilis* CspB (18) as well as for *L. monocytogenes* CspA (14) upon interaction with single-stranded DNA. We also have some indication that RNA binding is accompanied by a loss in local entropy at the binding interface. As has been reported by several authors before (13,39), the RNA-binding surface of cold shock proteins is characterized by a high degree of local mobility on the micro- to miliseconds time scale. This mobility is certainly required to accommodate nucleic acids of different type and structure by an induced-fit type interaction. Our ^{15}N CPMG-RD data recorded at 20°C indicate that these local dynamics are reduced (at least for the observable residues) pointing towards another entropic contribution to the binding affinity. At functionally relevant cold-shock temperatures, the entropic binding penalty is reduced, favoring CspA binding to RNA, but still resulting in relatively weak (μM range) binding affinities. This reduction in conformational entropy counterbalances the gain in free energy due to additional interactions at the protein–RNA interface. The transient character of the interaction provides the major driving force of the RNA chaperone activity without the requirement of external energy sources such as ATP consumption. It also presents a further example of an entropy transfer reaction that has been described as one of the characteristic properties of highly dynamic RNA chaperones, where the unfolding of the substrate is accompanied by an ordering of the chaperone protein itself (40).

Mechanisms of CspA's chaperone activity

The chaperone protein CspA mainly acts as a catalyzer of duplex formation by lowering the free energy barriers between the encounter complexes and the transition states (Figure 9B). This results in accelerated refolding kinetics, both for the fast and slow reaction pathways, but has no significant influence on the relative amplitudes (encounter complex formation) of the two kinetic phases. We assume that this chaperone activity is mainly due to the action of aromatic side chains on the surface of CspA that weaken RNA base pair interactions close to the interaction site, and thus speed up the zippering process that unfolds the RNA stem structure. In our RNA refolding assay, this effect is most pronounced for the thermodynamically more stable ACB hairpin where the loop nucleotides that are not in-

volved in hydrogen bonding interactions provide a suitable target for CspA binding, as discussed before. Base stacking interactions between the surface exposed aromatic CspA side chains and the loop nucleotide bases provide the required energy to destabilize the hydrogen bonds of the first two base pairs in the RNA stem. This destabilization effect then propagates through the whole stem, as demonstrated by the gradual decrease in the measured opening rate constants from the stem loop to the stem end. Similar, although less efficient chaperone activity is observed for CspA mutants either lacking one of the surface aromatics involved in the RNA interaction, or being structurally destabilized, and even for a simple aromatic tri-peptide. These findings indicate that the catalytic activity of aromatic residues is enforced by a favorable spatial arrangement as found on the surface of CspA.

Basic peptide residues also play an important role in RNA chaperone activity, mainly for compensating the negative charges on the RNA backbone, thus increasing the occurrence of encounter complex formation, as well as their lifetimes (reduced k_{off} rates). This also results in increased overall folding rates and, in the case of long peptide chains (poly-K), may also lead to a significant change in the relative amplitudes of the kinetic phases, most likely by increasing the occurrence of encounter complexes that have the right conformation for fast duplex formation. While this charge-compensation based RNA annealing activity is the main mechanism for the class of intrinsically disordered RNA chaperone proteins that possess a high percentage of basic residues (37), structured chaperone proteins, such as CspA, seem to have evolved to make use of the annealing power of both, aromatic and positively charged residues at the protein surface to efficiently bind and catalyze the restructuring of RNA. Still, RNA interactions with solvent-exposed positively charged or aromatic residues at the surface of proteins are sufficient for an unspecific RNA chaperone activity that might be important for a global cold adaption of the bacteria.

SUPPLEMENTARY DATA

Supplementary Data are available at NAR Online.

FUNDING

CEA; CNRS; University Grenoble Alpes; French National Research Agency [ANR-11-IS07-001]; Austrian Science Fund [I844, P26550, P28725]. We acknowledge access to the high-field NMR and *in-vitro* expression platforms of the Grenoble Instruct Centre (ISBG: UMS 3518 CNRS-CEA-UJF-EMBL) with support from FRISBI [ANR-10-INSB-05-02] and GRAL [ANR-10-LABX-49-01] within the Grenoble Partnership for Structural Biology (PSB). Funding for open access charge: CNRS.
Conflict of interest statement. None declared.

REFERENCES

1. Cristofari,G. and Darlix,J.-L. (2002) The ubiquitous nature of RNA chaperone proteins. *Prog. Nucleic Acids Res. Mol. Biol.*, **72**, 223–268.
2. Semrad,K. (2011) Proteins with RNA chaperone activity: a world of diverse proteins with a common task-impediment of RNA misfolding. *Biochem. Res. Int.*, 532908.
3. Rajkowitsch,L., Chen,D., Stampfl,S., Semrad,K., Waldsich,C., Mayer,O., Jantsch,M.F., Konrat,R., Bläsi,U. and Schroeder,R. (2014) RNA chaperones, RNA annealers and RNA helicases. *RNA Biol.*, **4**, 118–130.
4. Doetsch,M., Gstrein,T., Schroeder,R. and Fürtig,B. (2010) Mechanisms of StpA-mediated RNA remodeling. *RNA Biol.*, **7**, 735–743.
5. Godet,J., de Rocquigny,H., Raja,C., Glasser,N., Ficheux,D., Darlix,J.-L. and Mély,Y. (2006) During the early phase of HIV-1 DNA synthesis, nucleocapsid protein directs hybridization of the TAR complementary sequences via the ends of their double-stranded stem. *J. Mol. Biol.*, **356**, 1180–1192.
6. Bae,W., Phadtare,S., Severinov,K. and Inouye,M. (1999) Characterization of Escherichia coli cspE, whose product negatively regulates transcription of cspA, the gene for the major cold shock protein. *Mol. Microbiol.*, **31**, 1429–1441.
7. Phadtare,S. and Severinov,K. (2010) RNA remodeling and gene regulation by cold shock proteins. *RNA Biol.*, **7**, 788–795.
8. Giuliodori,A.M., Di Pietro,F., Marzi,S., Masquida,B., Wagner,R., Romby,P., Gualerzi,C.O. and Pon,C.L. (2010) The cspA mRNA Is a thermosensor that modulates translation of the cold-shock protein CspA. *Mol. Cell*, **37**, 21–33.
9. Jiang,W., Fang,L. and Inouye,M. (1996) The role of the 5'-end untranslated region of the mRNA for CspA, the major cold-shock protein of Escherichia coli, in cold-shock adaptation. *J. Bacteriol.*, **178**, 4919–4925.
10. Fang,L.I., Hou,Y.A.N. and Inouye,M. (1998) Role of the cold-box region in the 5 J untranslated region of the cspA mRNA in its transient expression at low temperature in Escherichia coli. *J. Bacteriol.*, **180**, 90–95.
11. Schindelin,H., Jiangt,W. and Inouye,M. (1994) Crystal structure of CspA , the major cold shock protein of Escherichia coli. *Proc. Natl. Acad. Sci. U.S.A.*, **91**, 5119–5123.
12. Mueller,U., Perl,D., Schmid,F.X. and Heinemann,U. (2000) Thermal stability and atomic-resolution crystal structure of the Bacillus caldolyticus cold shock protein. *J. Mol. Biol.*, **297**, 975–988.
13. Feng,W., Tejero,R., Zimmerman,D.E., Inouye,M. and Montelione,G.T. (1998) Solution NMR structure and backbone dynamics of the major cold-shock protein (CspA) from Escherichia coli: evidence for conformational dynamics in the single-stranded RNA-binding site. *Biochemistry*, **37**, 10881–10896.
14. Lee,J., Jeong,K.W., Jin,B., Ryu,K.S., Kim,E.H., Ahn,J.H. and Kim,Y. (2013) Structural and dynamic features of cold-shock proteins of Listeria monocytogenes, a psychrophilic bacterium. *Biochemistry*, **52**, 2492–2504.
15. Kremer,W., Schuler,B., Harrieder,S., Geyer,M., Gronwald,W., Welker,C., Jaenicke,R. and Kalbitzer,H.R. (2001) Solution NMR structure of the cold-shock protein from the hyperthermophilic bacterium Thermotoga maritima. *Eur. J. Biochem.*, **268**, 2527–2539.
16. Schnuchel,A., Wiltscheck,R., Czisch,M., Herrier,M., Willimsky,G., Graumann,P., Marahel,M.A. and Holak,T.A. (1993) Structure in solution of the major colld-shock protein from Bacillus subtilis. *Nature*, **364**, 169–171.
17. Max,K.E.A., Zeeb,M., Bienert,R., Balbach,J. and Heinemann,U. (2006) T-rich DNA single strands bind to a preformed site on the bacterial cold shock protein Bs-CspB. *J. Mol. Biol.*, **360**, 702–714.
18. Zeeb,M., Max,K.E.A., Weininger,U., Lo,C., Sticht,H. and Balbach,J. (2006) Recognition of T-rich single-stranded DNA by the cold shock protein Bs-CspB in solution. *Nucleic Acids Res.*, **34**, 4561–4571.
19. Sachs,R., Max,K.E.A., Heinemann,U. and Balbach,J. (2012) RNA single strands bind to a conserved surface of the major cold shock protein in crystals and solution. *RNA*, **18**, 65–76.
20. Phadtare,S., Inouye,M. and Severinov,K. (2004) The mechanism of nucleic acid melting by a CspA family protein. *J. Mol. Biol.*, **337**, 147–155.
21. Phadtare,S., Tyagi,S., Inouye,M. and Severinov,K. (2002) Three amino acids in Escherichia coli CspE surface-exposed aromatic patch are critical for nucleic acid melting activity leading to transcription antitermination and cold acclimation of cells. *J. Biol. Chem.*, **277**, 46706–46711.
22. Wunderlich,C.H., Spitzer,R., Santner,T., Fauster,K., Tollinger,M. and Kreutz,C. (2012) Synthesis of 6-13C-pyrimidine nucleotides as spin labels for RNA dynamics. *J. Am. Chem. Soc.*, **134**, 7558–75569.

23. Mok,K.H., Nagashima,T., Day,I.J., Jones,J.A., Jones,C.J. V, Dobson,C.M. and Hore,P.J. (2003) Rapid sample-mixing technique for transient NMR and photo-CIDNP spectroscopy: applications to real-time protein folding. *J. Am. Chem. Soc.*, **125**, 12484–12492.
24. Schanda,P., Forge,V. and Brutscher,B. (2007) Protein folding and unfolding studied at atomic resolution by fast two-dimensional NMR spectroscopy. *Proc. Natl. Acad. Sci. U.S.A.*, **104**, 11257–11262.
25. Schanda,P., Van Melckebeke,H. and Brutscher,B. (2006) Speeding up three-dimensional protein NMR experiments to a few minutes. *J. Am. Chem. Soc.*, **128**, 9042–9043.
26. Simorre,J.P., Zimmermann,F.R., Pardi,A., Farmer,B.T. and Mueller,L. (1995) Triple resonance HNCCCH experiments for correlating exchangeable and nonexchangeable cytidine and uridine base protons in RNA. *J. Biomol. NMR*, **6**, 427–432.
27. Simorre,J.P., Zimmermann,G.R., Mueller,L. and Pardi,A. (1996) Correlation of the guanosine exchangeable and nonexchangeable base protons in 13C-/15N-labeled RNA with an HNC-TOCSY-CH experiment. *J. Biomol. NMR*, **7**, 153–156.
28. Favier,A. and Brutscher,B. (2011) Recovering lost magnetization: polarization enhancement in biomolecular NMR. *J. Biomol. NMR*, **49**, 9–15.
29. Lee,D., Hilty,C., Wider,G. and Wüthrich,K. (2006) Effective rotational correlation times of proteins from NMR relaxation interference. *J. Magn. Reson.*, **178**, 72–76.
30. Tollinger,M., Skrynnikov,N.R., Mulder,F.A., Forman-Kay,J.D. and Kay,L.E. (2001) Slow dynamics in folded and unfolded states of an SH3 domain. *J. Am. Chem. Soc.*, **123**, 11341–11352.
31. Weininger,U., Respondek,M. and Akke,M. (2012) Conformational exchange of aromatic side chains characterized by L-optimized TROSY-selected ^{13}C CPMG relaxation dispersion. *J. Biomol. NMR*, **54**, 9–14.
32. Bouvignies,G. and Kay,L.E. (2012) Measurement of proton chemical shifts in invisible states of slowly exchanging protein systems by chemical exchange saturation transfer. *J. Phys. Chem. B*, **116**, 14311–14317.
33. Hwang,T.L., van Zijl,P.C. and Mori,S. (1998) Accurate quantitation of water-amide proton exchange rates using the phase-modulated CLEAN chemical EXchange (CLEANEX-PM) approach with a Fast-HSQC (FHSQC) detection scheme. *J. Biomol. NMR*, **11**, 221–226.
34. Schanda,P., Kupce,E. and Brutscher,B. (2005) SOFAST-HMQC experiments for recording two-dimensional heteronuclear correlation spectra of proteins within a few seconds. *J. Biomol. NMR*, **33**, 199–211.
35. Schanda,P. and Brutscher,B. (2005) Very fast two-dimensional NMR spectroscopy for real-time investigation of dynamic events in proteins on the time scale of seconds. *J. Am. Chem. Soc.*, **127**, 8014–8015.
36. Lescop,E., Rasia,R. and Brutscher,B. (2008) Hadamard amino-acid-type edited NMR experiment for fast protein resonance assignment. *J. Am. Chem. Soc.*, **130**, 5014–5015.
37. Ivanyi-nagy,R., Lavergne,J., Gabus,C., Ficheux,D. and Darlix,J.,2008) RNA chaperoning and intrinsic disorder in the core proteins of Flaviviridae. *Nucleic Acids Res.*, **36**, 712–725.
38. Phadtare,S. and Severinov,K. (2005) Nucleic acid melting by Escherichia coli CspE. *Nucleic Acids Res.*, **33**, 5583–5590.
39. Zeeb,M. and Balbach,J. (2005) NMR spectroscopic characterization of millisecond protein folding by transverse relaxation dispersion measurements. *J. Am. Chem. Soc.*, **127**, 13207–13212.
40. Tompa,P. and Csermely,P. (2004) The role of structural disorder in the function of RNA and protein chaperones. *FASEB J.*, **18**, 1169–1175.
41. Kupce,E. and Freeman,R. (1993) Polychromatic selective pulses. *J. Magn. Reson. A*, **102**, 122–126.
42. Geen,H. and Freeman,R. (1991) Band-selective radiofrequency pulses. *J. Magn. Reson.*, **93**, 93–141.